Characterization of Montmorillonite Biocomposite and Its Application for Trace Level Removal of Sb^{3+}: Equilibrium and Kinetic Studies

Ansar Anjum[1], Chand Kumar Seth[2] & Monika Datta[3]

[1] Department of Applied Science and Humanities, Galgotias' College of Engineering and Technology, Greater Noida- 201306, India.

[2] Department of Chemistry, Hindu College, University of Delhi, Delhi-110007, India.

[3] Department of Chemistry, University of Delhi, Delhi-110007, India.

Correspondence: Ansar Anjum, Department of Applied Science and Humanities, Galgotias' College of Engineering and Technology, Greater Noida- 201306, India. E-mail: ansaranjum_a@rediffmail.com

Abstract

The effluent from various industries is the potential source of water contamination during last few decades. Thus effective methods have been adopted for the removal of toxic heavy metals from industrial effluents that show carcinogenic and mutagenic effects. The present research involves removal of Sb^{3+} that has been investigated using chitosan-montmorillonite biocomposites. The kinetics and adsorption equilibrium was determined respectively using batch adsorption model, taking into account solution pH, contact time and initial metal ion concentration. The adsorption isotherm parameters were evaluated wherein Freundlich model best represents the experimental data. The highest adsorption capacity of 48.7 mg/g of chitosan-montmorillonite beads was attained from an initial concentration of 100 g/m^3 at 300 K. The equilibrium was achieved during initial phase of contact of 10 minutes only. The biosorbent show comparable high adsorption capacity for Sb^{3+} and is efficiently functional in broad range of metal ion concentration from 4 mg/m^3 (4 parts per billion) to 100 g/m^3 (100 parts per million) of solution. The adsorption kinetics follows chemical adsorption as the rate determining step.

The interaction forces between Sb^{3+} and adsorbent/s were determined by Fourier Transform Infrared-Attenuated Total Reflectance (FT-IR-ATR). The metal ion desorption and reusability of biosorbent/s up to three cycles was supported by 0.1 M potassium dihydrogen phosphate solution. The Scanning Electron Micrographs and X-Ray Diffractograms of the adsorbents before and after metal interaction were found to correspond to the batch adsorption studies of the metal ion.

Keywords: Sb^{3+}, adsorption, biosorbent, chitosan-montmorillonite, isotherm, kinetics, reusability

1. Introduction

Antimony is known to be a toxicological and carcinogenic metal. It is ubiquitously introduced to the environment from natural processes that include weathering of rock and soil run-off.

Human activities such as extensive use of lead alloys, battery grids, bearing metal, cable sheathing, plumber's solder, pewter, ammunition, sheet and pipe also add to the concentration of antimony in the environment. The total consumption of antimony in various industrial products is 1,00,000 tonnes per year worldwide. Among the most important uses of antimony in non-metal products are textiles, paints and lacquers, rubber compounds, ceramic enamels, glass and pottery abrasives, and certain types of matches [SbCl$_3$] (Ramesh, Hasegawa, Maki, Ueda, 2007). The metal, when discharged in wastewater represent a serious threat to human population. The concentrations of antimony in groundwater and surface water are found to be in the range of 0.1-0.2 mg/m^3 Hence the discharge of antimony into aquatic bodies and sources of drinking water has begun to be strictly controlled (Khan, Rasul, Munir, Habibuddowla, Alauddin, Newaz, & Hussam, 2000).

The bioavailability and toxicological effects of antimony depend on its chemical form and oxidation state (Haron, Rahim, Abdullah, Hussein, & Kassim, 2008). The two common inorganic forms of antimony in natural waters are, Sb^{5+}, [Sb (OH)]$^{6-}$ and Sb^{3+}, [Sb(OH)$_3$]. The toxicity of trivalent form of antimony, Sb^{3+} is ten times more than pentavalent form, Sb^{5+} (Mohanty, Majumder, & Mohanty, 2006). Its potential and proven carcinogenicity, immunotoxicity, genotoxicity, and reproductive toxicity makes the compounds of antimony to be considered as

pollutants of priority interest by the United States Environmental Protection Agency (USEPA), and the European Union (EU). The World Health Organization (WHO) guidelines limit the concentration of antimony as 0.005 g/L (5 mg/m^3) in drinking water (Monvisade and Siriphannon, 2009; Haque, Morrison, Jorge, & Torresday, 2008; Casariego, Souza, Cerqueira, Teixeira, Cruz, Dıaz, & Vicente, 2008). The increasing study on presence and behaviour of antimony in environment reflects the essential need to its remedy to be worked upon. The chronic toxicity of metal and the ecological demand for efficient removal of Sb^{3+} from parts per billion level in water has led us to make research for its remediation.

Adsorption and ion exchange, coagulation, flocculation and sedimentation, precipitation and microfiltration are the various conventional techniques reported for the removal of Sb^{3+} from aqueous solution (Rana, Halim, Waliul Hoque, Hasan, & Hossain, 2009; Jong & Stefan, 2008). Adsorption is observed to develop as a front line of defence for the remediation of antimony pollution. It has suitability for batch and continuous processes, effectiveness, ease of operation. It leads to little sludge generation and is economical and versatile in nature. The limited adsorption studies of antimony on natural sorbent have been reported till date, to the best of our knowledge. The adsorption capacity of Fe, Mn and Al hydroxides for Sb^{3+} indicates a decrease in the sequence from MnOOH > Al(OH)$_3$ > FeOOH (Antonio & Cestari, 2004; Nimrod & Mishael, 2010).

The present remediation methodology has not yet been reported for the removal of Sb^{3+}, (SbO$_3$)$^{3-}$ and to the best of our knowledge, the lowest detection limit of 1 g/m^3 has been reported by Xi, He & Lin (2011) using bentonite. The maximum adsorption efficiency is reported to be attained within contact time of 24 hours.

The objective of research is to develop a potent biosorbent that meets the ecological demands and is effective also at very low concentration, up to parts per billion of Sb^{3+} in water. Chitosan has been selected for the investigations since it is hydrophilic, biocompatible, biodegradable, and possess anti-bacterial property (Choudhari & Mahadevappa, 2009). At pH <5.5, chitosan forms gel that restricts its use as an adsorbent for Sb^{3+} from acidic industrial effluents. Hence, a natural occurring clay montmorillonite (Mt) has been used to treat chitosan to form composites. The treated chitosan is acid resistant and also provide higher surface area and stronger mechanical properties than pure chitosan. The adsorption of Sb^{3+} using synthesized biocomposites is likely to prevent widespread metal toxicity in nature.

Table 1. Characteristic properties of Sb^{3+} compound taken for studies (Potassium antimonyl tartrate)

Molecular Formula	K(SbO)C$_4$H$_4$O$_6$ .0.5H$_2$O
Empirical formula	C$_8$H$_4$ K$_2$O$_{12}$Sb$_2$. xH$_2$O
Molecular weight	613.83
Specific gravity	2.607
Solubility	In water 55 g/L at 20 ˚C
% Assay	99%
Colour	White

The modification of physical structure and chemical properties of chitosan using montmorillonite results in maximization of its adsorption capacity. Thus three chitosan treatments were investigated as well as the effect of pH, contact time and initial concentration on metal ion removal was studied. The feasibility of regeneration of sorbent after adsorption of Sb^{3+} was investigated using 0.1 M and 1 M sodium hydroxide, 0.1 M KH$_2$PO$_4$. A potential benefit of the study is the identification of a low cost, biocompatible, Sb^{3+} sensitive efficient sorbent for the removal of metal ions from aqueous solution. The work is a stepping stone to provide economical, easy and point-of-use systems for small communities and water utilities.

2. Materials and Methods

The clay mineral, Montmorillonite-KSF (Mt) was used in this study. The 2:1 layer mineral was obtained from Sigma Aldrich Pvt. Ltd. (Germany). Sodium hydroxide and hydrochloric acid were obtained from Qualingens (India). Leuco crystal violet (C$_{25}$H$_{31}$N$_3$) was obtained from Sigma Aldrich Pvt. Ltd. The stock solution of 250 g/m^3 Leuco crystal violet (LCV) was prepared in acidic medium in double distilled water. The volume of the solution was made up to 1000 ml in a standard volumetric flask. The solution was stable for several hours when kept in an amber flask away from the direct sunlight. Chitosan (Chi) was obtained from Everest Biotech.

Potassium antimonyl tartrate taken with 99% assay (Table 1), was obtained from Merck (India). Ortho-phosphoric acid was obtained from Merck (India). Sb^{3+} stock solution (1000 g/m^3) was prepared by dissolving 0.2668 g of potassium antimonyl tartrate in double distilled water. The volume of the solution was

made up to 1 L in a standard volumetric flask. The AR grade chemicals/reagents and double distilled water was used for the experiment.

2.1 Synthesis of Adsorbents

2.1.1 Chi-Mt Biocomposites

The biocomposite of Chi-Mt was synthesized by modifying the procedure reported previously by Jong and Stefan (2008). Chitosan was dissolved in 1 % (v/v) acetic acid under constant stirring for 4 hours to obtain chitosan solution. Mt was sieved, washed and dried at 80 ºC. The pH of chitosan solution was adjusted to ~ 5 using NaOH solution before adding to Mt suspension to avoid any structural variation of clay. The solution was then slowly added to the Mt suspension (2 %) at 323 K. The mixture was stirred for 24 hours and residue was finally washed with double distilled water until free from acetate ions. The residue thus obtained was dried at 323 K and labelled as Chi-Mt.

2.1.2 Beads of Chi and Chi-Mt

Chi and Chi-Mt beads were synthesized using 200 mg of chitosan flakes. The Chi flakes were allowed to stand overnight in 100 mL of 1 %(v/v) acetic acid. The resulting solution was added to a bath containing 0.5 M NaOH solution through a clinical syringe to form hydrogel beads. The chitosan hydrogel beads were allowed to stand in alkaline solution for 1 hour and then filtered and washed with double distilled water until the solution pH was neutral. The beads thus obtained were labelled as Chib.

Chi-Mt beads were synthesized using 200 mg of chitosan flakes and 300 mg of Mt. The mixture was allowed to stand overnight in 12 mL of 1 % (v/v) acetic acid. The resulting solution was added to a bath containing 0.5 M NaOH solution through a clinical syringe to form hydrogel beads. The Chi-Mt hydrogel beads were allowed to stand in alkaline solution for 1 hour and then filtered and washed with double distilled water until the solution pH was neutral and labelled as Chi-Mtb.
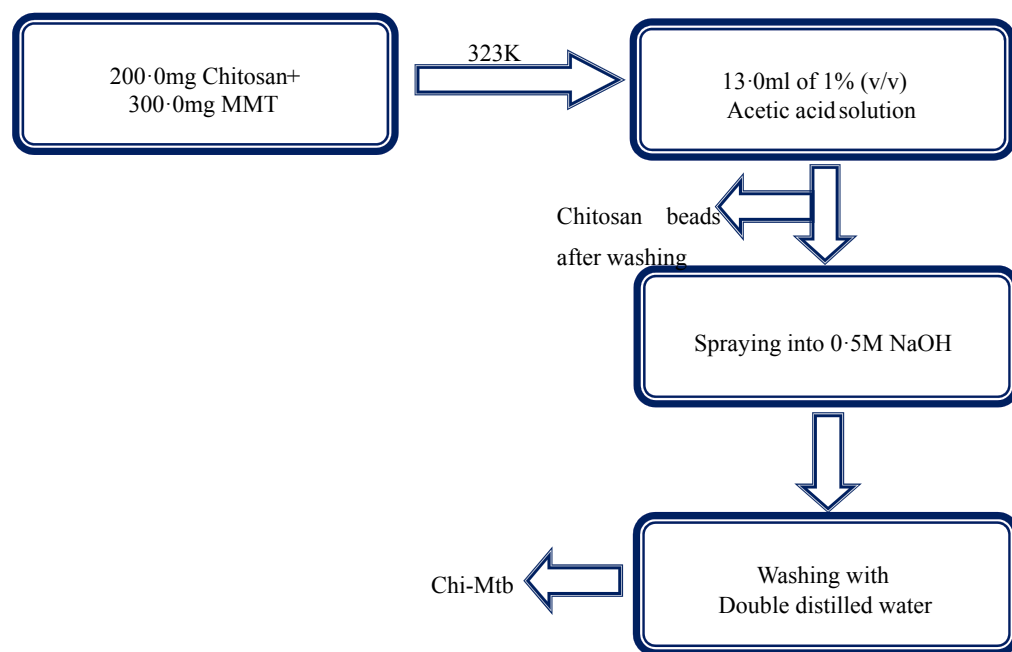

Figure 1. Schematic representation of synthesis of Chitosan Mt beads, Chitosan beads

2.2 Spectrophotometric Analysis

Quantitative estimation of Sb^{3+} was performed by UV-VIS spectrophotometric method using LCV as reported in the literature (Wong, Szeto, Cheung, & McKay, 2004). A rectilinear calibration graph (absorbance vs. concentration) of crystal violet (CV) was obtained at 592 nm by measuring the absorbance of solution over a known concentration range of Sb^{3+} as represented by the equation:

$$2IO_3^- + H_3SbO_3 + 2H^+ + LCV + OH^- \longrightarrow H_3SbO_4 + H_2O + CV^+ \text{ (Blue)}$$
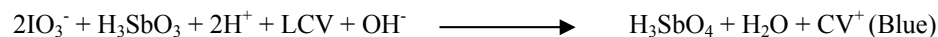
The batch adsorption studies were carried out as a function of pH, contact time and metal ion concentration.

0.1 g of the respective sorbent was exposed to 50 ml of $[SbO_3]^{3-}$ solution. The concentration of Sb^{3+} in the supernatant was estimated spectrophotometrically. The percentage of Sb^{3+} adsorbed onto the biosorbent was calculated using the equation 1.

$$\%Adsorption = \left[\frac{(C_i - C_e)}{C_i}\right] \times 100 \qquad (1)$$

Amount of Sb^{3+} adsorbed (q_e) was calculated from the relationship

$$q_e = \left(C_i - C_e\right) \times V \div m \qquad (2)$$

where C_i represents initial Sb^{3+} concentration (mg/L) and C_e the final Sb^{3+} concentration in the solution after equilibrium was attained (mg/L), V is the volume of the Sb^{3+} solution (mL) and m is the mass of the adsorbent (mg) used.

3. Results and Discussion

3.1 Removal of Sb^{3+} as a Function of pH

The important factor that affects removal of Sb^{3+} is pH of metal ion solution. The effect of pH on removal of Sb^{3+} on Chi and its biocomposites was investigated in the pH range of 2–8, using adsorbent doze of 2 g/L, at 20 ˚C. The behaviour of Sb^{3+} towards chitosan based adsorbents could be explained by pK_a of chitosan that is 5.6. Thus, Chib was restricted from removing Sb^{3+} from the solution by charge neutralization. The adsorption of Sb^{3+} using Chib may be a function of hydrogen bond formation or *Van der Waals* force between pH 4-9, thereby supporting the application of Chib and Chi-Mtb for removal of Sb^{3+} in broad range of pH.

The Chib were found to be highly unstable in acidic range and thus no considerable data could be obtained at pH less than 4. The removal of Sb^{3+} was observed to be a pH independent phenomenon beyond pH range of 5 for Chib and during pH range of 5 – 9 for Chi-Mt. The adsorption of metal ion upon Chib decreases from 96.4 % at pH 6 to 95.8 % at pH 7 (figure 2A). The adsorption of metal ion increases from 79 % at pH 2 to 95.5 % at pH 7 upon Chi-Mt. Due to insignificant difference in Sb^{3+} removal, pH 5-6 appeared to be the optimal range for efficient adsorption of Sb^{3+}. No significant decrease in Sb^{3+} adsorption was observed until the pH >9 under the experimental conditions. At pH <4, the amount of Sb^{3+} removed from solution is found to decrease. The free amine groups probably present on the external surface as well as in the interlayer of Chi-Mt were responsible for the adsorption of specie from water. The neutral and negatively charged Sb^{3+} ions present at pH >9 are attracted to the positively charged surface of the adsorbent thereby resulting in sufficient Sb^{3+} adsorption.

The Chi-Mtb show 94.4 % removal efficiency at pH 2 that increased to 97.5% at pH 6 as represented in figure 2A. In aqueous solution Sb^{3+} is present as $[SbO]^+$ and $[Sb(OH)_2]^+$ species at pH < 3. Neutral $[HSbO_2]$ and $[Sb(OH)_3]$ species are predominant at pH 3–10 that onsets dissociation with increasing pH to produce $[SbO_2]^-$ species (Thanabalasingam & Pickering, 1990). At pH < 2, competition of abundantly available positively charged hydronium ions adds up that causes decreased adsorption capacity of adsorbent. Thus competitive binding between hydronium ions and antimony species, $[SbO]^+$ and $[Sb(OH)_2]^+$ is present to the surface of biosorbent.

At pH > 6, decrease in adsorption of Sb^{3+} is due to competition for the sorption sites between hydroxyl ions and hydroxylated complexes of Sb^{3+}. The adsorption maxima at around pH 6 can be explained by the fact that the difference between the energy released upon adsorption and energy required to dissociate the acid is at a maximum.

Similar results have also been reported for the sorption of antimony on metal-loaded saponified orange waste, goethite (α-FeOOH) and activated alumina (Duarte, Ciminelli, Dantas, Duarte, Vasconcelos, Oliveira, & Osseo-Asare, 2012; Weerasooriya, Tobschall, Wijesekara, Arachchige, & Pathirathne, 2003).

3.2 Removal of Sb^{3+} as a Function of Contact Time

The effect of contact time on the amount of Sb^{3+} removed from aqueous solution was investigated during 1-120 minutes as shown in figure 2A. The Chi was observed to show an increase in Sb^{3+} removal from 93% during the initial contact time of 10 minutes to 96% at 60 minutes. An increase in removal of metal ion from 90.5% during initial 10 minutes to 97.5% at 60 minutes was observed using Chi-Mtb.

Chi-Mt shows an increase in adsorption of Sb^{3+} from 91.6% during 10 minutes to 95.5% during 60 minutes. A steep rise in Sb^{3+} removal was observed during the initial contact time of 1-10 minutes as shown in figure 2 due to the availability of a large number of adsorption sites on the adsorbent surface.

The equilibrium was investigated by exposing the Sb^{3+} ions for contact time of 10, 20, 30, 40, 50, 60, 70, 80, 90, 100, 120 minutes respectively. The constant removal of metal ion was observed within 70 minutes. To investigate the change in removal capacity of adsorbents the batch studies were extended up to 120 minutes.

3.3 Equilibrium Studies of Sb^{3+} Adsorption

The adsorption capacity of biosorbents increased with an increase in initial metal ion concentration. The maximum removal of 97.5 % observed from 100 g/m^3 aqueous Sb^{3+} concentration using Chi-Mtb (figure 2B) after which no further increase in adsorption was observed due to nearly complete coverage of the sorption sites of biosorbents at high initial concentration of Sb^{3+}. At lower metal ion concentrations, the ratio of initial number of Sb^{3+} ions to the available adsorption sites is low, whereas at higher concentrations, the number of available adsorption sites becomes lower, and subsequently the removal of Sb^{3+} ions depend on the initial concentration.

The Chib shows an increase in adsorptive removal of metal ion from 87 % to 96.4 % on increase in initial metal ion concentration from 10-100 g/m^3. The removal of Sb^{3+} from an initial concentration of 0.1 g/m^3 was observed to decrease to 40%. The Chi-Mtb shows an increase in adsorption of Sb^{3+} from 91 % to 97.5 % with an increase in concentration of metal ion from 10-100 g/m^3. It shows an adsorption of 50.3 % from an initial concentration of 0.1 g/m^3.

The increase in adsorption of Sb^{3+} within the given concentration range indicates a heterogeneous system wherein adsorption is not restricted to monolayer formation. The adsorption capacity of Sb^{3+} using Chi-Mtb was observed to be higher than Chib as well as the pristine Mt as reported by Anjum and Datta (2012). The Chi-Mt shows an increase in adsorption from 87.6 % to 95.5 % with an increase in concentration of metal ion from 10 -100 g/m^3 (figure 2B). The biosorbent has also been found to possess the efficiency to remove almost 75 % of Sb^{3+} from an initial concentration of 0.1 g/m^3. The trace level removal of Sb^{3+} from 0.008 g/m^3 shows 42 % removal using Chib, 34 % removal using Chi-Mt, and 46 % removal using Chi-Mtb respectively. The zetametry (+30 mV for Chi-Mt and +10 mV for Mt) suggest electrostatic attraction between the positively charged adsorbent and negatively charged adsorbate. The increased in adsorption potential of Chi-Mtb may be attributed to increase in surface area of spherical beads and incorporation of the characteristics of Mt and chitosan as well.

The Langmuir isotherm did not show a good linear fit as can be seen from isotherm parameters in Table 1. This implies that Sb^{3+} adsorption is not monolayer and independent adsorbent sites are occupied by every metal ion only during initial phase of adsorption. Maximum adsorption capacity calculated using this model was observed to be 11.9 mg/g, and 1.77 mg/g using Chi-Mt and Chi-Mtb was respectively. This capacity is much less in magnitude when compared with the Freundlich isotherm model.

Table 2. Adsorption isotherm parameters for Sb^{3+} adsorption on Chib, Chi-Mt, and Chi-Mtb.

Model Parameters	Chib	Chi-Mt	Chi-Mtb
Langmuir isotherm			
q_m *(mg/g)*	1.7	11.9	1.8
K_l *(l/mg)*	5.7	4.0	14.1
R^2	0.67	0.70	0.67
Freundlich isotherm			
K (mg/g)	44.2	48.9	50.0
1/n	1.0	0.8	0.6
R^2	0.98	0.98	0.99

The Freundlich adsorption isotherm shows no apparent plateau for the range of concentrations studied indicating the effectiveness of biosorbents for the adsorption of metal ion. The experimental data shows a satisfactory fit to Freundlich isotherm (better than the Langmuir isotherm fit) particularly for adsorption on Chi-Mtb followed by Chi-Mt and somewhat less so on Chib as can be seen from table 2.

The Freundlich isotherm constant depicts higher sorption affinity of metal ion for Chi-Mtb (n=1.67) followed by Chi-Mt (n=1.25). The least affinity for Sb^{3+} is shown by Chib (n=1). This agrees well with the batch extraction studies that shows maximum adsorption efficiency of the order Chi-Mtb > Chi-Mt. The adsorption efficiency of Chi-Mt (50.3 %) was observed to be 25 % more than Chi-Mtb (75 %) from initial concentration of as low as 0.1 g/m^3. Thus, Sb^{3+} adsorption was observed to follow the order Chi-Mtb > Chi-Mt > Chib. The maximum adsorption capacities calculated from Langmuir isotherm was found to be in the order Chi-Mt > Chi-Mtb > Chib as shown in table 2. However the adsorption capacity of biosorbents obtained from Langmuir isotherm was appreciably less. The isotherm shows a poor regression coefficient (R^2 = 0.67, 0.67 and 0.70 respectively for Chi-Mtb, Chib, and Chi-Mt). The goodness of the fit of experimental data measured by the determination coefficients, R^2 shows Freundlich isotherm as the best model for adsorption of Sb^{3+} using biosorbents.

Table 3. Comparison of Sb^{3+} sorption capacity of montmorillonite-biocomposite with different sorbents.

| Sorbent	Sorption capacity (mg/g)	Reference
Chemically bonded adsorbent	21.92	Deorkar and Tavlarides (1997)
Goethite (-FeOOH)	61.2 (average value)	Watkins, Weiss, Dubbin, Peel, Coles, and Arnold (2006)
Hydrous oxide of Mn	17.05	Thanabalasingam and Pickering (1990)
Hydrous oxide of Fe	12.18	Thanabalasingam and Pickering (1990)
Diatomite	35.2	Ahmet, Demirhan, and Mustafa (2010)
Mt-Chi beads	48.7	Present study
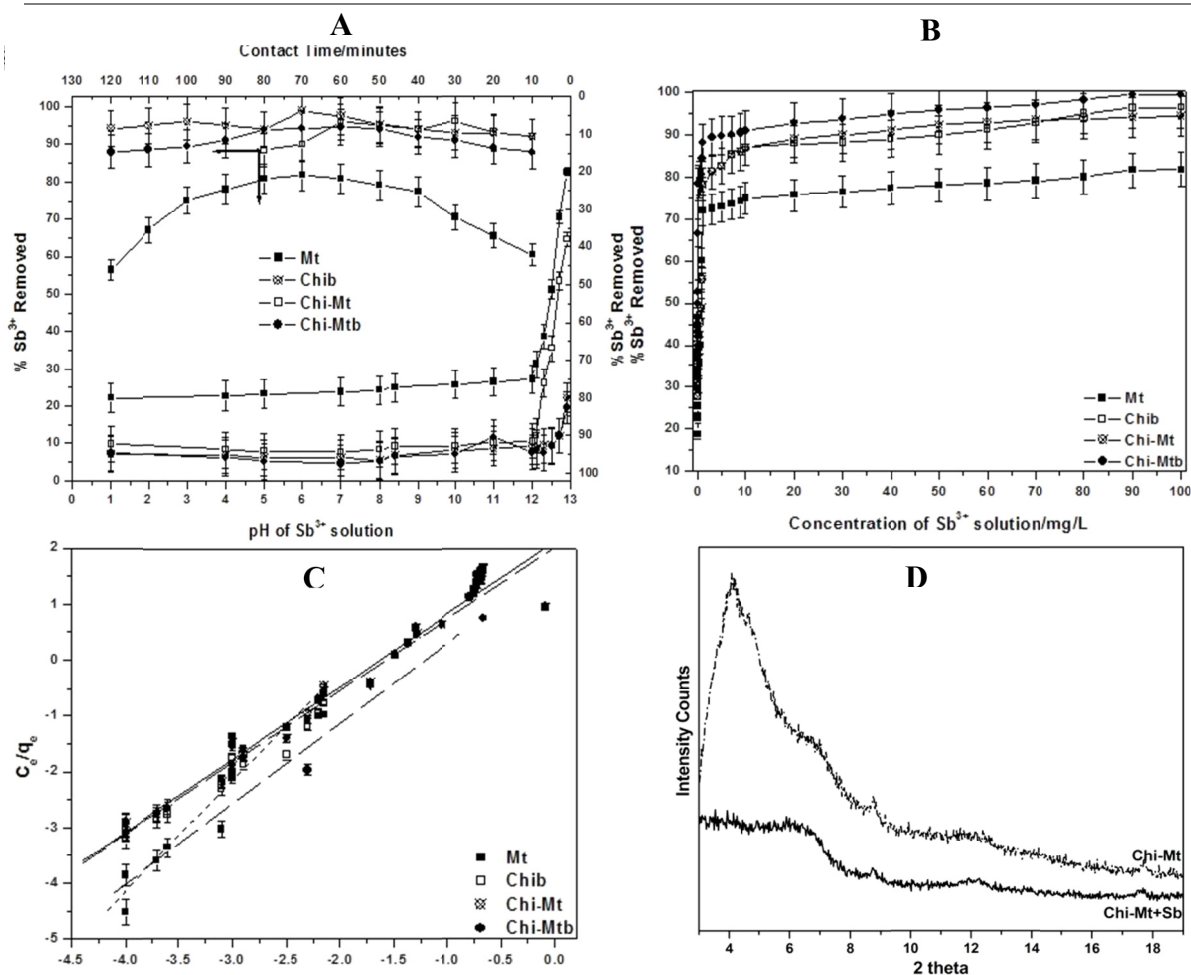
Figure 2. A plot of Adsorption efficiency of biosorbents as a function of A- pH and contact time with Sb^{3+} ions in solution, $[Sb^{3+}] = 100 \text{ g/m}^3$ at 300 K; B- Initial concentration of Sb^{3+} ions, pH = 6, contact time = 60minutes at 300 K; C- Freundlich adsorption isotherm; D- X-ray diffractogram of Chi-Mt before and after adsorption of Sb^{3+} ions.

A decrease in values of "n" with the change in biosorbent from Chi-Mtb to Chib indicates that Sb^{3+} ions are favourably and efficiently adsorbed by Chi-Mtb at room temperature. Chi-Mtb shows a good capacity of Sb^{3+} adsorption from water up to parts per billion level that has not been approached so far (table 3) to the best of our knowledge thus, making the adsorbent to be used commercially in future for efficient extraction of Sb^{3+} from water.

4. Characterization of Biosorbents

4.1 X-ray Diffractometry

The X-ray diffractogram of Mt, Chi-Mtb and the respective biosorbents were obtained with Cu-K_α radiation (1.544 Å). The intercalation of chitosan has been observed in phyllosilicate as also evident from the diffractogram. The $d_{(001)}$ spacing of Mt was observed to be 12.0 Å.

An increase in $d_{(001)}$ spacing of Mt is observed that is due to the movement of chitosan into the interlayer gallery causing an increase of 9.2 Å with respect to Mt. The broad reflection around 2θ value of 6.8° (d_{001} 12.96 Å) as shown in figure 2 was assumed to be due to monolayer of chitosan in the interlayer gallery of Mt whereas $d_{(001)}$ 22.2 Å was related to the intercalation of chitosan bilayers as reported by Monvisade and Siriphannon (2009). The interaction of Mt with Sb^{3+} ions made a shift of $d_{(001)}$ diffraction peak towards lower 2theta values from 6·10° to 5·38° indicating the expansion of basal spacing to 17 Å (an increase of 4Åwith respect to Mt). This could be attributed to the movement of metal ion into the interlayer gallery of Mt thereby causing an increase in the basal spacing. This is due to the presence of large number of NH_3^+ sites in the network of the biopolymer that accommodates an appreciable number of the metal ions that makes the basal spacing to increase. The disappearance of the chitosan peak at 18° has been found to disappear after Sb^{3+} adsorption.

The 2theta value was found to decrease from 5.02° to 2.89° on interaction of Chi-Mt with Sb^{3+} ions. This corresponds to an increase in basal spacing to 31.2Å. The $d_{(001)}$ diffraction peak at 6.70° was found to shift to 5.06° and an increase in basal spacing to 21.2Å as shown in figure 2D. Thus, the observed decease in diffraction $d_{(001)}$ peak value points towards an intercalation of Sb^{3+} into the interlayer gallery of Chi-Mt that contributes to the extraction efficiency of the adsorbents for Sb^{3+}. As evident from the diffractograms the basal spacing depends on the amount of the available moiety intercalated and varies from one adsorbent to another. Thus, the order of intercalation corresponds well with the adsorption efficiency of the adsorbents as obtained by the batch adsorption studies. The intercalation of Sb^{3+} in Mt was possibly due to the availability of freely accessible intergallery space. Therefore it can be deduced that some Sb^{3+} ions are expected to move into the interlayer gallery which in conjunction with adsorption on the other sites consequently result in greater Sb^{3+} adsorption capacity and also corresponds to the spectrophotometric studies.

4.2 Fourier Transform-Infra Red-Attenuated Total Reflectance Analysis

The FT-IR-ATR spectrum of Mt after Sb^{3+} interaction at optimized pH and contact time shows the presence of small peak at around 1454 $cm^{-1}$and 866 cm^{-1} respectively that corresponds to the stretching vibrations of Sb-O bond. The Si-O stretching vibration (1047 cm^{-1}) was found to shift to lower wavenumber at 1038 cm^{-1}. The O-H bending vibration (1641 cm^{-1}) was found to shift to higher wavenumber at 1656 cm^{-1} that reflect the interaction of Sb^{3+} with the hydroxyl group of Mt. The O-H stretching vibration (3600 cm^{-1}) was found to shift to lower wavenumber at 3582 cm^{-1} respectively that reflect the presence of hydrogen bonded O-H group possibly with the adsorbate present in the solution (Sb^{3+}).

The N-H bending vibration of protonated amino groups (1632 cm^{-1}) in Chib was observed to be shifted to a higher wavenumber at 1638 cm^{-1} after interaction with Sb^{3+} suggesting ionic attraction between $R'- NH_3^+$ and $(SbO_2)^-$ group as well as possible hydrogen bonding between antimony and –OH group of chitosan. The C-O-C stretching vibration in Chib (1148 cm^{-1} and 1033 cm^{-1}) shifted to lower wavenumber at 1071 cm^{-1} and 1029 cm^{-1} respectively after interaction with Sb^{3+} due to formation of bidentate inner complex of Sb^{3+} with oxygen of C-O-C groups (adjacent to C1 and C5) of chitosan. However, a new stretching vibration at 1360 cm^{-1} has been observed possibly due to presence of Sb-O bond (figure3).

The N-H bending vibration frequency 1543 cm^{-1} (NH_2 vibration of protonated amino groups) of Chi-Mtb after interaction of $Sb^{3+}$with the N-H bending vibration frequency 1543 cm^{-1} (NH_2 vibration of protonated amino groups) $(SbO_2)^-$ was found to disappear suggesting the ionic attraction between $R'- NH_3^+$ and $(SbO_2)^-$ group. The shift in the frequency of stretching vibration of Si-O and C-O-C (overlapping band at 1023 cm^{-1}) in Chi-Mtb to higher frequency (1037 cm^{-1}) after interaction with Sb^{3+} and has been interpreted as due the formation of bidentate inner complex of Sb^{3+} with oxygen of C-O-C and Si-O groups. The 911 cm^{-1} band assigned to the Al-O stretching vibration of the biosorbent is not observed after interaction with Sb^{3+}, suggesting a likely shift in the vibrational frequency beyond 650 cm^{-1}.

After the interaction of Chi-Mt with Sb^{3+} the overlapping Si-O and C-O-C stretching vibration (1023 cm^{-1}) have been found to shift to higher frequency at 1055 cm^{-1} and has been interpreted as due to the formation of a chemical bond (inner sphere complex formation by Sb^{3+} and oxygen of the ring (C-O-C) and oxygen on the surface of the clay. The overlapping bands of O-H and N-H stretching vibration have been observed to shift to a higher frequency (3625 cm^{-1} to 3630 cm^{-1}) after interaction with Sb^{3+}. The shift in Al-O stretching vibration was observed to a lower wavenumber at 622 cm^{-1} after Sb^{3+} interaction that suggest chemical interaction between Sb^{3+} and Al-O group at the edges of clay particles. The N-H bending vibration frequency (1630 cm^{-1}) of protonated amino groups (at C2') has been found to shift to a higher wavenumber at 1642 cm^{-1} after interaction of Sb^{3+}. After interaction of Chi-Mt with metal ion a new peak was observed at 885 cm^{-1} and 728 cm^{-1} that signifies the possibility of presence of Sb-O bond.

The reduction in peak wavenumber, a new peak as a result of splitting of the initial peak is indicative of chemical bonding or an inner-sphere complex. The basic role in the formation of Sb^{3+}-chitosan compound has been played by

amino and hydroxyl groups. A shift in the $-NH_3$ vibration has been reported after Sb^{3+} interaction that is indicative of the chelation of metal ion by chitosan. Thus, it has been supported that $-NH_3^+$ systems are dominantly responsible for metal extraction properties and the application of the ad sorbents as active phase for Sb^{3+} extraction and detection. This also explains the possible ionic attraction between $R'-NH_3^+$ and SbO_2^- groups. The peak at 2886 cm $^{-1}$ is due to C–H stretching vibration of $-CH_2$ and $-CH_3$ groups of chitosan. The bands and relative intensities for Sb^{3+} sorption on the adsorbents are found to be concentrated between 1400 cm^{-1} and 600 cm^{-1} as represented in figure 3. Since a shift in $-NH_3$ vibration has been reported when chelation of metal ion by chitosan takes place. Thus, it has been corroborated that $-NH_3^+$ systems are responsible for exchange properties and the application of Chi-Mt, Chib, and Chi-Mtb as active phase for its detection. The surface complex model theory (STUM) states that the metal hydroxyl groups on the surface of adsorbents are the reactive adsorption sites for anions. The interaction of Sb^{3+} on the surface of adsorbent with hydroxyl group can be represented as: Step (i) represents Sb^{3+} adsorption on the surface as monodentate ligand exchange and step (ii) represents bidentate ligand exchange of Sb^{3+} with hydroxyl group that involve chemical bond formation.

Though the ionic attraction between the sorbent and sorbate is the dominant mechanism, factors such as and diffusion of sorbate into the polymers are to be considered plausible uptake mechanisms. Thus, the mechanism involved in Sb^{3+} removal from an aqueous medium through adsorption onto the biosorbents may be due to one or a combination of several factors such as (1) ionic attraction, (2) physical adsorption, and (3) absorption. At pH 6, the predominant Sb^{3+} species present in aqueous medium is uncharged H_3SbO_3 and negatively charged $H_2SbO_3^-$ which undergo electrostatic interaction with the adsorbent. However, such species can interact with the unprotonated amino groups and some hydroxyl groups in the biosorbent may involve in coordination with the adsorbate as also supported by the FT-IR-ATR spectrum.

4.3 Thermogravimetry (TGA – DTA)

The Mt shows a decrease in weight loss (from 18.6 % to 1 %) that accounts to the decrease in physisorbed water. This is attributed to the presence of Sb^{3+} possibly by replacement of surface water molecules in the temperature range from 10 °C–102 °C after Sb^{3+} adsorption. The second step weight loss in the temperature range from 105 °C to 261 °C was found to decrease (from 10.7 % to 5.1 %) whilst the third weight loss was observed to be 57 % in the temperature range from 320 °C to 820 °C corresponding to an endotherm at 350 °C in DTA possibly due to presence of metal ion. An exotherm at 620 °C (37 % weight loss) in DTA due to structural OH loss was observed leaving behind 37 % residue. The residue left after Sb^{3+} interaction was found to decrease (53 % in MMT) and therefore can be said to depict the presence of metal.
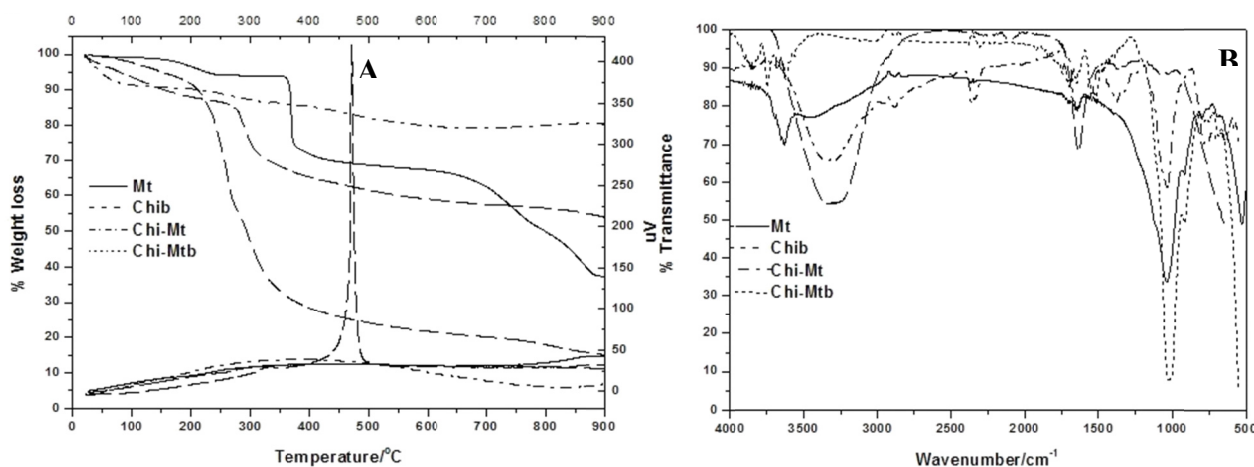

Figure 3. A plot of A-TGA-DTA analysis of biosorbents after adsorption of Sb^{3+} B- FT-IR-ATR spectrum of biosorbents after adsorption of Sb^{3+}.

A weight loss of 5 % has been observed in Chib due to physisorbed water followed by consecutive second and third weight loss of around 62 % possibly due to chitosan correspondingly at 284 ºC in DTA leaving behind 21 % residue. The Chi-Mtb and Chi-Mt show respective first step weight loss of 5 % and 7 % in the temperature range from 20 ºC-106 ºC that corresponds to an exotherm at 28 ºC in Chi-Mtb and at 26 ºC in Chi-Mt in DTA. The second step weight loss in Chi-Mtb and Chi-Mt was observed to be 37 % and 13 % respectively in the temperature range from 110 ºC to 775 ºC that corresponds to an exotherm at 318 ºC in Chi-Mtb and an endotherm at 317 ºC in DTA leaving behind 57.3 % residue in Chi-Mtb isotherm whereas 79 % residue in Chi-Mt respectively due to the presence of chitosan and antimony.

4.4 Scanning Electron Microscopy

The biosorbents after interaction with Sb^{3+} show an appreciable change in morphology of the adsorbents as shown in figure 4. Since the more porous adsorbents provides increased surface area for efficient extraction of Sb^{3+} thus, after the metal ion adsorption the reduced porosity of the adsorbents further proves the successful metal treatment that provides a less porous morphology to the natural and synthesized biosorbents. The scanning micrographs reveals smooth, homogenous and densely-packed morphology of the matrices that may be attributed to the presence of adsorbed species onto the porous structure, probably to the bound Sb^{3+}. The transmission electron micrograph shows diameter of shows that diameter of Chi-Mt after Sb^{3+} ranges from 10-20.3 nm respectively.
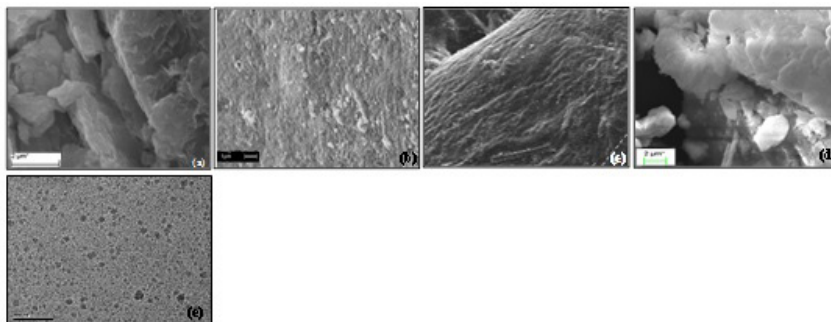

Figure 4. Scanning electron micrographs of (a) MMt (b) Chi-Mtb (c) Chib (d) Chi-Mt after adsorption of *Sb^{3+}*

(e) Transmission electron micrograph of Chi-Mt after Sb^{3+} adsorption.

4.4 Kinetics of Sb^{3+} Adsorption

The mechanism of Sb^{3+} removal using the three biosorbents and the potential rate controlling step has been subjected to extensive research. A steep rise in rate of metal ion removal was observed during initial contact time of 10 minutes after which the rate slowed down as the equilibrium is approached.

The comparison of best fit sorption mechanism of Sb^{3+} on Chi-Mtb, Chi-Mt, and Chib were made with 100 g/m³ of Sb^{3+} using 2 g/L of adsorbent dose. The overall calculation for the rate of adsorption of Sb^{3+} was estimated and the mechanism of adsorption was determined by the rate determining step. Lagergren's pseudo-first order model for the adsorptive extraction of Sb^{3+} has been investigated. The rate equation for the liquid/solid system based on solid capacity[15] has the linear form of equation 3.

$$\log[q_e - q_t] \equiv \log q_e - \frac{k_1}{2.303} \times t \qquad (3)$$

This kinetic model assumes that the rate of change of solute uptake is directly proportional to the difference in saturation concentration and the amount of solute uptake. The linear fit correlation coefficient (R^2) of log ($q_1 - q_t$) against t for Sb^{3+} adsorption on Chi-Mtb, Chi-Mt, and Chib as shown in figure 5 were found to be 0.78, 0.98 and 0.87 respectively. The results indicate that Sb^{3+} adsorption does not totally agree for the strict first order adsorption mechanism and thus deviates the pseudo–first-order reaction model slightly particularly on Chi-Mt and Chib. Thus, physisorption is said to be accompanied with another model related to pore diffusion.

Ho and Mckay pseudo-second order kinetic model is based on the sorption capacity of the solid phase and is represented by equation 4.

$$\left[\frac{t}{q_t}\right] \equiv \frac{1}{k_2 * q_e^{\,2}} \oplus \frac{1}{q_e} * t \qquad (4)$$

This model states that chemisorption may be the rate limiting step of the sorption system involving valence forces through sharing or exchange of electrons between sorbent and sorbate.

The model shows the linear correlation coefficient (R^2) values to be 0.98 for Chib, 0.99 for Chi-Mtb and 0.99 for Chi-Mt (figure 5). Chi-Mtb and Chi-Mt show favourable adsorption coefficient indicating that the adsorptive extraction of Sb^{3+} involves chemical bond formation with the respective biosorbents favourably following the pseudo second order model as also supported by the FT-IR-ATR studies.

A possibility of transport of Sb^{3+} into the interlayer space and pores of biosorbent/s has been observed due to attiring on batch process as also supported by the experimental coefficient correlation of pseudo first order reaction model. This possibility was investigated in terms of Weber and Morris Intraparticle diffusion model that depicts a graphical relationship between the amount of Sb^{3+} adsorbed and square root of time as depicted by equation 5.

$$[q_t] \equiv k_p * \sqrt{t} \qquad (5)$$

Weber and Morris model show multilinearity that signifies the Sb^{3+} adsorption as a two or more steps mechanism. Initially the graph appears to be sharper and replicates instantaneous adsorption stage of Sb^{3+} onto the external surface of adsorbent. The experimental results show a steep rise in instantaneous adsorption of Sb^{3+} onto Chi-Mtb and Chi-Mt during this stage whereas Chib shows a gradual rise with less amount of instantaneously adsorbed Sb^{3+}.

The second stage represents gradual adsorption stage of Sb^{3+} wherein intraparticle diffusion of the metal ion into interlayer gallery of Chi-Mt and the pores of Chib and Chi-Mtb is rate controlled. The pore diffusion of Sb^{3+} in graphical representation shows steep rise in Chib, Chi-Mtb, and Chi-Mt. This could be due to the enhanced porous morphology. In the third stage a plateau is approached that represents final equilibrium stage of Sb^{3+} removal wherein the intraparticle diffusion starts to slow down due to extremely low concentration of Sb^{3+} left in the solution. The linear parts of the curves do not appear to pass through origin, indicating that the mechanism of adsorptive extraction of Sb^{3+} using biosorbents is a complex phenomenon wherein both surface chemisorption as well as intraparticle diffusion contributes to the rate determining step.
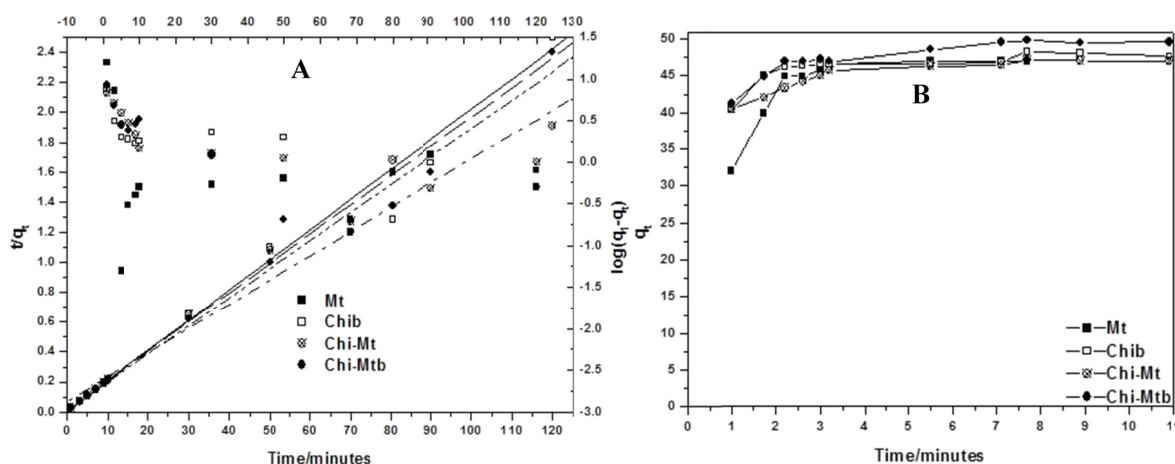

Figure 5. A plot of **A**-Pseudo-first order and Pseudo-second order kinetic models **B**- Intraparticle diffusion model for biosorbents, $[Sb^{3+}] = 100$ g/m^3 at 300 K.

The larger the intercept, the greater is the contribution of external mass transfer that was found to be in the order Chib > Chi-Mt > Chi-Mtb. Thus, it suggests that a greater portion of Sb^{3+} extraction using Chib involves diffusion into the pores whereby Chi-Mtb involves extraction through chemical bond formation/chemisorption as well as intraparticle diffusion of Sb^{3+} through pores.

Table 4. Kinetic equations for Sb^{3+} adsorption onto biosorbents

Adsorbent + Sb^{3+}	Time/ Minutes	Models of reaction	Equation of linear fit	k (Exp)	k (Calc)	R^2
Mt	01-10	Pseudo-first order	ln (q$_e$-q$_t$)= 1·34 - 0·457t	1·03	1·10	0·697
	01-10	Intraparticle diffn	q$_t$= 7·95 t$^{0.5}$ − 25·74	7·95	1·00	0·928
	10-120	Pseudo-second order	t/q$_t$ = 0·0106 + 0·021t	0·040	0·044	0·996
Chi-Mtb	01-10	Pseudo-first order	ln (q$_e$-q$_t$)= 0·54+0·011t	0·030	0·341	0·773
	01-10	Intraparticle diffn.	q$_t$= 0·623 t$^{0.5}$ + 45·3	0·623	1·28	0·811
	10-120	Pseudo-second order	t/q$_t$= 0·0132+0·0199t	0·03	0·08	0·999
Chib	01-10	Pseudo-first order	ln (q$_e$-q$_t$)= 0·477 -0·084t	0·200	0·205	0·865
	01-10	Intraparticle diffn.	q$_t$= 0·44 t$^{0.5}$ + 45·1	0·44	2·34	0·686
	10-120	Pseudo-second order	t/q$_t$=0·0137+0·0195t	0·028	0·22	0·999
Chi-Mt	01-10	Pseudo-first order	ln (q$_e$-q$_t$)= 0·923 -0·070t	0·161	0·231	0·988
	01-10	Intraparticle diffn·	q$_t$= 0·566 t$^{0.5}$ − 42·2	0·566	1·20	0·837
	10-120	Pseudo-second order	t/q$_t$= -0·0027+0·0215t	0·17	0·09	0·931

4.5 Desorption and Reusability Studies of Biosorbents

The reusability of biosorbents was investigated by consecutive five adsorption–desorption cycles using the same respective sorbent. Desorption of Sb^{3+} using 0.1 M NaOH during optimized contact time of 600 minutes was

performed repeatedly to investigate the reusability of adsorbent. The desorption of Sb^{3+} from Mt was observed to be 28 % that decreased up to 4 % during five cycles whereas the adsorption efficiency of Mt was observed to decrease from 82% to 23% in the second cycle. The total amount of Sb^{3+} retained after five cycles was observed to be 2.123 mg. The percentage of Sb^{3+} desorbed from Chi-Mtb was observed to increase from 21 % to 49 % during the contact time of 60 minutes and 720 minutes respectively. The desorption of Sb^{3+} from Chib was observed to increase from 33% to 64% with the increase in contact time of 60 minutes and 600 minutes respectively. The percentage of Sb^{3+} desorbed from Chi-Mt was observed to increase from 13 % to 48 % during the contact time of 60 minutes and 600 minutes respectively.

The desorbent medium of 0.1 M KH_2PO_4 shows desorption efficiency of 39% of Sb^{3+} when Mt (Sb^{3+} adsorbed) were subjected to it during the first cycle. The Chi-Mtb and Chib were observed to show desorption of 49 % and 64 % Sb^{3+} respectively when the metal ion adsorbed adsorbents were exposed to the desorbent medium. After first desorption cycle the adsorbent was again exposed to 100 g/m^3 of Sb^{3+} solution wherein the adsorption capacity of Chi-Mtb and Chib decreased 99 % to 33 % and 96 % to 49 % respectively during the second cycle as shown in figure 5. The Chi-Mt shows a desorption competence of 48 % of Sb^{3+} on exposing to the desorbent medium. The adsorption capacity of Chi-Mt was observed to decrease from 95 % to 20 % during the second cycle. The total amount of Sb^{3+} retained after five cycles was observed to be by 2.981 mg using Chi-Mt, 2.871 mg using Chi-Mtb, and 2.757 mg using Chib respectively (figure 6). The mass action and diffusion processes might effect Sb^{3+} desorption from poorly accessible Sb^{3+} adsorption sites. Apparently, some sites have very strong affinity for Sb^{3+} and show slow desorption kinetics even at high desorbent concentrations and high P: Sb molar ratios.

The readsorption Sb^{3+} on surface of biosorbent decreases due to increased -OH concentration and increased competition for ligand-exchange sites. The rate of ligand exchange would be enhanced by protonation of oxygen at the Fe-O-Sb sites, resulting in reduced strength of Sb^{3+} bonding at the iron oxide surface of Mt. After an initially rapid Sb^{3+} desorption, the rate of desorption by phosphate decreased with either increasing reaction time or sequential extraction due to lack of ease of accessibility of adsorption sites or different metal ion bonding strengths at different adsorption sites. The competition between antimony and phosphate is influenced by mass action and diffusion of phosphate concentration; however, desorption of the metal ion from some adsorption sites occurs very slowly, even at high phosphate concentration. Although Sb^{3+} desorption efficiency of biosorbents is highly dependent on initial phosphate concentration but considerable antimony is still retained in the presence of high phosphate concentration also. Hence, complete ligand exchange between phosphate and antimony could be achieved.

These studies indicate that low antimony-extraction efficiency by phosphate could be attributed to both a slow kinetics of arsenic exchange and very strong retention of some Sb^{3+} at adsorption sites. Also, poor accessibility of Sb^{3+}, which might be trapped by soil aggregates, could also influence the low efficiency of Sb^{3+} extraction. The vitality of the biosorbents for the application of removal of Sb^{3+} is their recurrent availability for Sb^{3+} adsorption through many cycles of adsorption/desorption from aqueous solution. The high stability of Chi-Mt and Chi-Mtb allowed three cycles of adsorption/desorption process. Based on these results, it can be concluded that Chi-Mt and Chi-Mtb prove to be as competitive adsorbent with respect to the adsorption performance after a large number of sorption/desorption cycling.
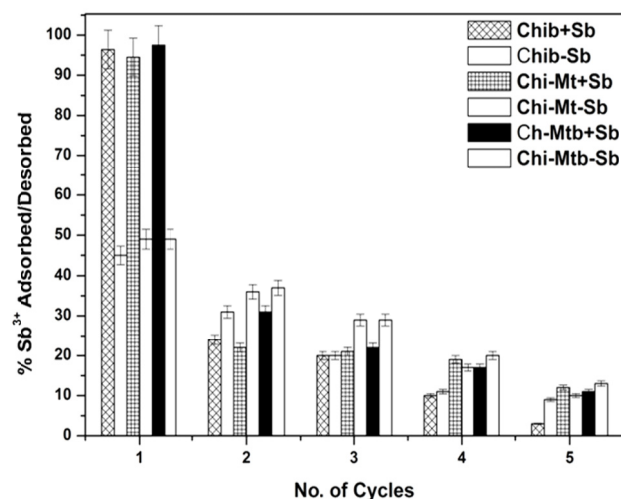

Figure 6. A plot of percentage of Sb^{3+} adsorbed/desorbed versus number of cycles

5. Conclusions

The maximum extent of Sb^{3+} adsorption depends on pH and is highest in the pH range of available drinking water due to the speciation of Sb^{3+}. A quantitative prediction of Sb^{3+} adsorption to natural materials is however, a challenging task mainly due to its inherent complexity, particularly with respect to surface heterogeneity. In this study the adsorption mechanism was examined. It was observed that a variety of other processes, in particular interactions/and redox transformation of Sb^{3+} with natural organic matter contribute to overall sorption in nature. The information obtained from the results here should provide essential first step in efficient extraction of the most toxic arsenic specie from aquatic systems.

The adsorptive extraction efficiency of the biocomposites investigated at very low concentration of metal ion was found to be dynamically sensitive up to four parts per billion of Sb^{3+}. The biocomposites have been found to be sensitive to very dilute solution of metal ion concentration up to 0.008 g/m^3. The Chi-Mtb show promising behaviour for the removal of trace levels of Sb^{3+} from water. The analyte undergoes instantaneous adsorption onto the surfaces that is responsible for adsorptive extraction during initial phase of contact. The surface complexation of Sb^{3+} with the adsorbent further enhances the adsorption capacity of the analyte onto the adsorbents during later phase of extraction. This phenomenon was observed to be well supported by the kinetic studies. The higher adsorptive extraction on Chi-Mtb may be explained by the high total surface area resulting from spherical shape of beads and the increased porous nature due to containing interlinked channels.

The batch extraction results have been well supported by FT-IR-ATR analysis of the adsorbents after Sb^{3+} adsorption that indicate surface complexation between –OH, -NH sites and Sb^{3+} respectively rather than solid phase precipitation that may add to a large amount of sludge generation.

Thus, the integration of Chitosan with Montmorillonite has proved to enhance the extraction capacity of the pure Chitosan as an adsorbent for the removal of toxic metal from water.

Acknowledgments

References

An, J. H., & Stefan, D. (2008). Adsorption of Cr (VI) and As (V) on chitosan-montmorillonite: selectivity and pH dependence. *Clays and Clay Minerals, 56*(5), 549–557. http://dx.doi.org/10.1016/j.microc.2007.08.004.

Anjum, A., & Monika, D. (2012). Adsorptive Removal of Antimony (III) Using Modified Montmorillonite: A Study on Sorption Kinetics. *Journal of Analytical Sciences, Methods and Instrumentation, 2,* 167-175. http://dx.doi.org/10.4236/jasmi.2012.23027.

Antonio, R., Cestari, A., Eunice F. S., Vieira, Aline G. P., Jackeline A. M., & Vanessa, P. de A. (2004). Adsorption of anionic dyes on chitosan beads. 1. The influence of the chemical structures of dyes and temperature on the adsorption. *Journal of Colloid and Interface Science, 280,* 380–386. http://dx.doi.org/10.1016/j.jcis.2004.08.007.

Bleiman, N. B., & Mishael, Y. G. (2010). Selenium removal from drinking water by adsorption to chitosan–clay composites and oxides: Batch and columns tests. *Journal of Hazardous Materials, 183,* 590–595. http://dx.doi.org/10.1016/j.jhazmat.2010.07.065

Casariego, A., Souza, B. W. S., Cerqueira, M. A., Teixeira, J. A., Cruz, L., Díaz, R., & Vicente, A. A. (2009). Chitosan/clay films' properties as affected by biopolymer and clay micro/nanoparticles' concentrations. *Food Hydrocolloids, 23,* 1895–1902. http://dx.doi.org/10.1016/j.foodhyd.2009.02.007

Choudhari, S. K., & Mahadevappa, Y. K. (2009). Development of novel composite membranes using quaternized chitosan and Na^+-MMT clay for the pervaporation dehydration of isopropanol. *Journal of Colloid and Interface Science, 338,* 111–120. http://dx.doi.org/10.1016/j.jcis.2009.05.071

Deorkar, N. V., & Tavlarides, L. L. (1997). A chemically bonded adsorbent for separation of antimony, copper and lead. *Hydrometallurgy, 46,* 121–135. http://dx.doi.org/10.1016/s0304-386x(97)00006-6

Duarte, G., Ciminelli, V. S. T., Dantas, M. S. S., Duarte, H. A., Vasconcelos, V., Oliveira, A. F., & Osseo-Asare, K. (2012). As (III) immobilization on gibbsite: Investigation of the complexation mechanism by combining EXAFS analyses and DFT calculations. *Geochimica et Cosmochimica Acta, 83,* 205–216. http://dx.doi.org/10.1016/j.gca.2011.12.019

Haque, N., Morrison, G. A., Jorge, L. G., & Torresday. (2008). Iron-modified light expanded clay aggregates for the removal of arsenic (V) from groundwater. *Microchemical Journal, 88*(1), 7-13.

http://dx.doi.org/10.1016/j.microc.2007.08.004

Haron, M. J., Rahim, F. A., Abdullah, A. H., Hussein, M. Z., & Kassim, A. (2008). Sorption removal of arsenic by cerium-exchanged zeolite P. *Materials Science and Engineering B, 149*(2), 204-208. http://dx.doi.org/10.1016/j.mseb.2007.11.028

Xi, J., He, M., & Lin, C. (2011). Adsorption of antimony(III) and antimony(V) on bentonite: Kinetics, thermodynamics and anion competition. *Microchemical Journal,* 97(1), 85-91. DOI: 10.1016/j.microc.2010.05.017

Khan, A., Rasul, S. B., Munir, A. K. M., Habibuddowla, M., Alauddin, M., Newaz, S. S., & Hussam, A. (2000). Appraisal of a simple arsenic removal method for ground water of Bangladesh. *Journal of Environmental Science and Health, Part A, 35*(7), 1021-1041. http://dx.doi.org/10.1080/10934520009377018

Maiti A., DasGupta, S., Basu, J. K., & De, S. (2007). Adsorption of arsenite using natural laterite as adsorbent. *Separation and Purification Technology*, *55*(3), 350-359. http://dx.doi.org/10.1016/j.seppur.2007.01.003

Mondal, P., Majumder, C. B., & Mohanty, B. (2006). Laboratory based approaches for arsenic remediation from contaminated water: Recent developments. *Journal of Hazardous Materials, 137*(1), 464-479. http://dx.doi.org/10.1016/j.jhazmat.2006.02.023

Monvisade, P., & Siriphannon, P. (2009). Chitosan intercalated montmorillonite: Preparation, characterization and cationic dye adsorption. *Applied Clay Science, 42,* 427–431. http://dx.doi.org/10.1016/j.clay.2008.04.013

Ramesh, A., Hasegawa, H., Maki, T., & Ueda, K. (2007). Adsorption of inorganic and organic arsenic from aqueous solutions by polymeric Al/Fe modified montmorillonite. *Separation and Purification Technology, 1*, 90-100. http://dx.doi.org/10.1016/j.seppur.2007.01.025

Rana, M. S., Halim M. A., Waliul H. S.A.M., Hasan K., & Hossain M.K. (2009). Bioadsorbtion of arsenic by prepared and commercial crab shell chitosan. *Biotechnology, 8*(1), 160–165. http://dx.doi.org/10.3923/biotech.2009.160.165

Sarı, A., Cıtak, D., & Tuzen, M. (2010). Equilibrium, thermodynamic and kinetic studies on adsorption of Sb(III) from aqueous solution using low-cost natural diatomite. *Chemical Engineering Journal, 162,* 521–527. http://dx.doi.org/10.1016/j.cej.2010.05.054

Thanabalasingam, P., & Pickering, W. F. (1990). Specific sorption of antimony (III) by the hydrous oxides of Mn, Fe, and Al. *Water Air and Soil Pollution, 49*, 175–185. http://dx.doi.org/10.1007/BF00279519

Watkins, R., Weiss, D., Dubbin, W., Peel, K., Coles, B., & Arnold, T. (2006). Investigations into the kinetics and thermodynamics of Sb(III) adsorption on goethite (α-FeOOH). *Journal of Colloid and Interface Science*, *303*, 639–646. http://dx.doi.org/10.1016/j.jcis.2006.08.044

Weerasooriya, H. J., Tobschall, H. K. D. K. Wijesekara, E. K. I. A. U. K. Arachchige, & K. A. S. Pathirathne. (2003). On the mechanistic modeling of As (III) adsorption on gibbsite. *Chemosphere*, *51*, 1001–1013. http://dx.doi.org/10.1016/s0045-6535(03)00157-7

Wong, Y. C., Szeto, Y. S., Cheung, W. H., & McKay, G. (2004). Pseudo-first-order kinetic studies of the sorption of acid dyes onto chitosan. *Journal of Applied Polymer Science, 92*, 1633–1645. http://dx.doi.org/10.1002/app.13714

Copyrights